AIAA JOURNAL
Vol. 33, No. 11, November 1995

New Similarity Solutions for Hypersonic Boundary Layers with Applications to Inlet Flows

George R. Inger*
Iowa State University, Ames, Iowa 50011–3231

A re-examination of self-similar solution possibilities for steady laminar boundary layers is given for nonadiabatic strongly hypersonic flows of an ideal gas. Two apparently new solutions are found, pertaining to adverse pressure gradients, both of which involve no separation with distance into the pressure rise. The first involves an exponential pressure rise on a cooled similarly shaped body, whereas the second involves a modified ramp type pressure rise. The skin friction, heat transfer, displacement thickness, and weak viscous interaction-induced pressure change properties of these two solution families are analyzed in detail, including their application to high-speed inlet type of flows.

Nomenclature

C_f = skin friction coefficient, $2\tau_w/\rho_\infty U_\infty^2$
C_h = heat transfer coefficient, Eq. (21)
C_p = specific heat
C_w = Chapman–Rubesin parameter, $\mu_w T_\infty/\mu_\infty T_w$
C_1 = constant in pressure distribution, Eq. (18)
f = boundary-layer similarity stream function, Eq. (3)
f_p = $(2p_e/p_\infty)/\gamma(\gamma+1)M_\infty^2$, Eq. (26)
G = similarity transformation function, Eq. (1)
g = boundary-layer total enthalpy function, H/H_e
H = total enthalpy, $c_pT + u^2/2$
I_g = $\int_0^\infty (g - f'^2)\,d\eta$, Eq. (22)
K_B = $M_\infty \sin\theta_B$, Eq. (24)
K_G = similarity coefficient, Eq. (7)
L = arbitrary reference length
$\mathcal{L}$ = function defined in Eq. (30)
M = Mach number
N = power law exponent in $p_e \sim x^N$
Pr = Prandtl number
P_0 = stagnation pressure, Eq. (34)
p = static pressure
$\dot{q}_w$ = wall heat transfer rate
Re_L = Reynolds number, $\rho_\infty U_\infty L/\mu_\infty$
T = absolute static temperature
u = streamwise velocity component in boundary layer
x, y = Cartesian coordinates along and normal to wall
$\hat{x}, \hat{y}$ = $x/L, y/L$
x_0 = origin of inlet body pressure rise, Fig. 9
y_B, y_{Beff} = actual and effective ($y_B + \delta^*$) body shape
β = exponential similarity coefficient as in $p_e \sim e^{\beta x}$; see Eqs. (10–13)
γ = specific heat ratio
δ^*, δ = displacement thickness and boundary-layer thickness, respectively
η = boundary-layer similarity coordinate, Eq. (1)
θ_B = body slope angle
λ = parameter defined in Eq. (14)
μ = coefficient of viscosity
ξ = transformed x coordinate; see Eq. (2)
ξ_{ref} = $\rho_\infty \mu_\infty C_w U_\infty L$
$\hat{\xi}$ = ξ/ξ_{ref}
ρ = density
τ_w = wall shear stress
$\bar{\chi}$ = $M_\infty^3\sqrt{(C_w/Re_{\infty L})}$, viscous-inviscid interaction parameter
$()'$ = $d()/d\eta$

Subscripts

CR = see Eq. (16)
e = conditions at boundary-layer edge
eff = effective body shape
w = conditions along body surface
∞ = freestream conditions

Introduction

A SIGNIFICANT aspect of the aerodynamic design of planned spaceplane hypersonic vehicles is the use of integrated airframe/propulsion wherein the aircraft forebody acts as a precompression surface for the engine inlet. Consequently, the details of the boundary-layer development and heat transfer effects on this forebody (which occurs in an adverse pressure gradient approaching the inlet) are of crucial concern in understanding the inlet conditions. Notwithstanding the existence of powerful Euler/Navier–Stokes computer codes for predicting such flows, it is still desirable to supplement these tools with basic analytical concepts that explain and correlate the purely numerical results and that also may reveal new ideas about improving the aerodynamic design. The present work addresses this issue by seeking some new laminar boundary-layer solutions for hypersonic adverse pressure gradient flows that are pertinent to the high-speed inlet problem.

Although self-similar solutions for slender hypersonic bodies of power law shape and their corresponding boundary layers are well known,[1] the existence of another type of such similarity solution in the case of exponentially shaped bodies is not generally appreciated (Fig. 1). To date, however, only the inviscid aspect of this exponential family has been explored.[2] Since the inviscid field involved is one of an adverse pressure gradient in the streamwise direction, the question of whether the corresponding underlying boundary-layer behavior is also self-similar (and, if so, its nature) is not only of intrinsic fundamental interest but is also relevant to the aforementioned engine inlet flow application. The present paper describes a detailed study of this question and its application value to the engineering design and computational fluid dynamics (CFD) simulation of strongly hypersonic inlet flows.

Formulation of the Analysis

We confine attention to steady laminar flow of a perfect gas in which the motion is regarded as two dimensional (the extension to axisymmetric flow, if desired, is quite straightforward via the Mangler transformation[3]). To bring out the essential physics of interest

Presented as Paper 94-2351 at the AIAA 25th Fluid Dynamics Conference, Colorado Springs, CO, June 20–23, 1994; received June 21, 1994; revision received May 24, 1995; accepted for publication May 30, 1995.

*Professor, Department of Aerospace Engineering and Engineering Mechanics. Associate Fellow AIAA.

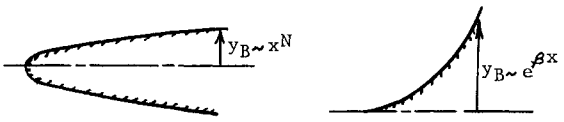

a) Power law b) Exponential

Fig. 1 Body shapes for inviscid hypersonic similarity solutions.

here, the transport properties are sufficiently approximated by Stewartson's model gas[4] ($\rho\mu = \text{const} = \rho_w\mu_w$ and $Pr = 1$ across the boundary layer). We further consider the case of strongly hypersonic small-disturbance inviscid flow in the limit where $M_\infty^2 \gg 1$, $U_e \cong U_\infty$, and $H_e \cong U_e^2/2$; see Ref. 3. Finally, for the purposes of this first phase of study, we shall neglect the effects of strong viscous-inviscid interaction, although we later discuss its implications. It is noted that arbitrary wall heat transfer is allowed in the analysis, assuming a constant but arbitrary wall to total temperature ratio.

Under the aforementioned simplifying assumptions, we then introduce the generalized coordinate transformation

$$\eta = \frac{U_e}{G}\int_0^y \rho\,\mathrm{d}y \tag{1}$$

$$\xi = \xi(x) \tag{2}$$

where the choice of the functions ξ and $G(\xi)$ is subsequently determined by similarity requirements. We also introduce the usual nondimensional dependent variables

$$u/u_e = f'(\eta) \tag{3}$$

$$H/H_e = g(\eta) \tag{4}$$

where $H = c_pT + u^2/2$ is the total enthalpy. Then the boundary-layer momentum and energy equations take the following form under the tentative assumption of self-similar motion (f and g functions of η only) for constant pressure across the boundary layer:

$$\left(\frac{\mathrm{d}G/\mathrm{d}\xi}{G}\right)ff'' + K_G f''' = \frac{\mathrm{d}u_e/\mathrm{d}\xi}{u_e}\left(f'^2 - \frac{\rho_e}{\rho}\right) \tag{5}$$

$$\left(\frac{\mathrm{d}G/\mathrm{d}\xi}{G}\right)fg' + K_G g'' = 0 \tag{6}$$

where

$$K_G \equiv \frac{\rho_w\mu_w u_e}{G^2\mathrm{d}\xi/\mathrm{d}x} = C_w\rho_\infty\mu_\infty U_\infty\left(\frac{p_e/p_\infty}{G^2\mathrm{d}\xi/\mathrm{d}x}\right) \tag{7}$$

and $C_w = \mu_w T_\infty/\mu_\infty T_w$ is the Chapman–Rubesin constant. The attendant boundary conditions on the solution to Eqs. (5) and (6) are $f'(\infty) = g(\infty) = 1$ to match with the inviscid flow at the outer edge of the boundary layer as $\eta \to \infty$, and the no-slip conditions on the impermeable wall are $f(0) = f'(0) = 1$ and $g(0) = c_pT_w/H_e$, where T_w is arbitrary.

It is convenient for the present purposes to express the right-hand side of Eq. (5) in terms of g and the inviscid pressure gradient. To do this we first utilize the equation of state (with $\partial p/\partial\eta = 0$) and the inviscid energy equation $H_e = c_pT_e + U_e^2/2$ to obtain

$$\frac{\rho_e}{\rho} \cong \frac{T}{T_e} = \frac{H_e g}{c_pT_e} - \frac{U_e^2}{2c_pT_e}(f')^2 = g + \left(\frac{H_e}{c_pT_e} - 1\right)(g - f'^2) \tag{8}$$

Then applying the inviscid Euler equation $\rho_e U_e \mathrm{d}U_e = -\mathrm{d}p_e$ and equation of state, use of Eq. (8) renders the right side of Eq. (5) into the following form upon using the hypersonic approximation $H_e \cong U_e^2/2$:

$$\frac{\mathrm{d}U_e/\mathrm{d}\xi}{U_e}\left(f'^2 - \frac{\rho_e}{\rho}\right) \cong \left(\frac{\gamma - 1}{2\gamma}\right)\frac{\mathrm{d}p_e/\mathrm{d}\xi}{p_e}(g - f'^2) \tag{9}$$

Assessment of the Similarity Solution Possibilities

Equations (5) and (6) reduce to a set of ordinary differential equations when the coefficient of each η-dependent term is constant; this occurs in the following four unique cases upon taking $K_G = \mathrm{d}G/G\mathrm{d}\xi$.

Case 1:

$$\xi = x, \qquad G \sim x^{(1+N)/2}, \qquad p_e \sim x^N \tag{10}$$

Case 2:

$$\xi = C_w\rho_\infty\mu_\infty U_\infty\int_0^x\left(\frac{p_e}{p_\infty}\right)\mathrm{d}x, \qquad G \sim \xi^{\frac{1}{2}}, \qquad p_e \sim \xi^N \tag{11}$$

Case 3:

$$\xi = x, \qquad G \sim e^{\beta x/2}, \qquad p_e \sim e^{\beta x} \tag{12}$$

Case 4:

$$\xi = \ln\left[1 + C_w\rho_\infty\mu_\infty U_\infty\int_0^x\left(\frac{p_e}{p_\infty}\right)\mathrm{d}x\right], \qquad G \sim e^{\xi/2}, \qquad p_e \sim e^{\beta\xi} \tag{13}$$

The first case corresponds to the classical Howarth–Dorodnitzn (H–D) transformation, and the second to the so-called[3] Levy–Lees (L–L) transformation: both pertain to self-similar flows around slender hypersonic power law bodies in strongly hypersonic flow[3] and result in Eqs. (5) and (6) reducing to the well-known ordinary differential equations solved and extensively tabulated by Cohen and Reshotko.[5] On the other hand, cases 3 and 4 are apparently new and clearly correspond to exponential types of inviscid flow; case 3 involves the H–D transformation with a physically exponential pressure rise, whereas case 4 entails a kind of exponential L–L transformation with an interesting pressure distribution as shown subsequently.

Confining attention hereafter to compressive flows $\beta > 0$, the aforementioned new cases yield from Eqs. (5–9) the pair of governing boundary layer equations,

$$ff'' + f''' = \lambda\left(\frac{\gamma - 1}{\gamma}\right)(g - f'^2) \tag{14}$$

$$fg + g'' = 0 \tag{15}$$

where $\lambda = 1$ for case 3, whereas $\lambda = \beta$ for case 4 [see Eq. (18)]. We realize with delight that these equations and their boundary conditions correspond exactly to those already studied by Cohen and Reshotko[5] in the adverse pressure gradient regime if we merely

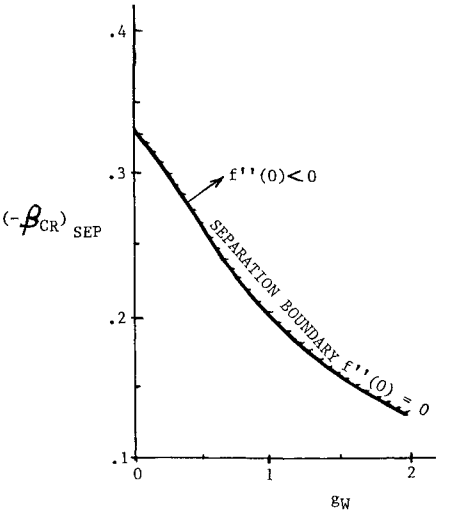

Fig. 2 Adverse pressure gradient parameter for separation.

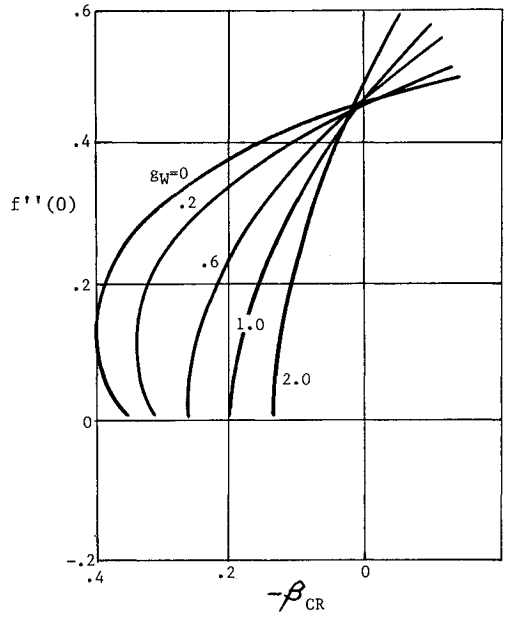

Fig. 3 Wall shear function $f''(0)$ for self-similar solutions with adverse pressure gradient (Ref. 5).

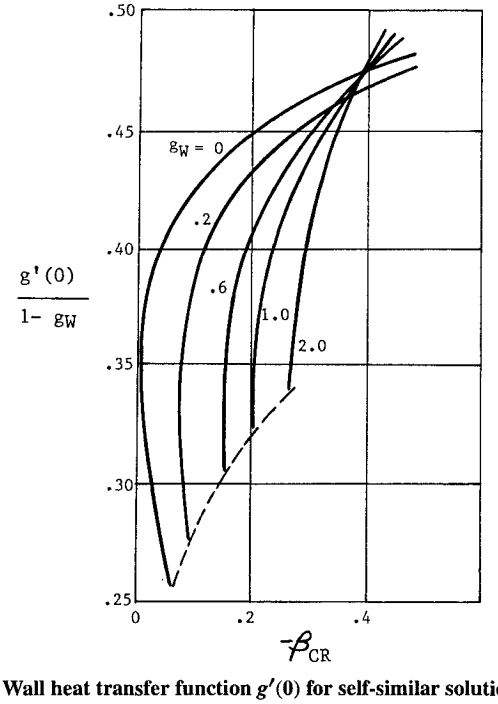

Fig. 4 Wall heat transfer function $g'(0)$ for self-similar solutions with adverse pressure gradient (Ref. 5).

equate their pressure gradient parameter (β_{CR}, say) to the present one by the relationship

$$\beta_{CR} = -\lambda(\gamma - 1)/\gamma \tag{16}$$

Provided we restrict attention to the regime of solutions with nonreversed flow [$f''(0) \geq 0$] whose boundary is delineated by a wall temperature-dependent value of β_{CR} as shown in Fig. 2, the present new solutions therefore require no numerical work at all and can be evaluated by a direct adaptation of known tabulated results!

Figures 3 and 4 show the values so obtained for the basic shear stress and wall heat transfer similarity functions $f''(0)$ and $g'(0)$, respectively, as functions of β_{CR} and the wall temperature ratio. It will be noted that double-valued nonseparated solutions are obtained for $-\beta_{CR} > -0.26$ if the wall is sufficiently cooled ($g_w < 0.6$); the reason for this nonunique behavior lies in the history of flow development near the leading edge, as discussed by Cohen and Reshotko.[5]

Physical Properties of the New Similarity Solution

Pressure Distribution

By inverting the aforementioned transformations, we can extract the various physical properties of direct engineering interest. To facilitate this process, it is convenient to introduce an arbitrary characteristic length L and associated dimension $\xi_{ref} = \rho_\infty \mu_\infty C_w U_\infty L$ with corresponding nondimensional independent variables and $\hat{x} \equiv x/L$ and $\hat{\xi} \equiv \xi/\xi_{ref}$, respectively. Then after some algebra, the new similarity solutions yield the following results. The pressure distributions along the flow for case 3 are given by

$$p_e/p_\infty = K_{p_1} e^{\beta\hat{x}} = K_{p_2} e^{\beta(\hat{x}-\hat{x}_0)} \tag{17}$$

and for case 4 by

$$p_e/p_\infty = K_{p_3}[1 + C_1(1-\beta)(\hat{x} - \hat{x}_0)]^{\beta/(1-\beta)} \tag{18}$$

where the $K_{p_{1,2,3}}$ plus C_1 and x_0 are all arbitrary parameters. Whereas Eq. (17) is obviously an exponential pressure rise (Fig. 1a) and associated with a cusped concave exponential ramp (see below), Eq. (18) describes a mixed ramp/power law type of pressure rise (Fig. 5), which with its four disposable parameters is especially attractive as a model of the pressure rise on a preinlet compression surface.

Skin Friction and Heat Transfer

Using the values $G = \sqrt{(2K_{p_1}\xi_{ref}/\beta)}\, e^{\beta\hat{x}/2}$ for case 3 and $G = \sqrt{(2\xi_{ref}K_{p_3})}\exp(\hat{\xi}/2)$ for case 4, the corresponding skin friction distributions are found to be for case 3:

$$C_f \equiv \frac{2\mu_w(\partial u/\partial y)_w}{\rho_\infty U_\infty^2} = \frac{2\rho_w\mu_w}{\rho_\infty G} f''(0)$$

or

$$C_f \equiv \sqrt{2\beta K_{p_1} C_w/Re_L}\; e^{\beta\hat{x}/2} f''(0) \tag{19}$$

and for case 4:

$$C_f = \sqrt{2K_{p_3}^{1/\beta} C_w/Re_L}\left(\frac{p_e}{p_\infty}\right)^{(2\beta-1)/2\beta} f''(0) \tag{20}$$

whereas for $Pr = 1$ the heat transfer coefficients are both obtained from the common relationship that

$$C_h = \frac{2\mu_w(\partial H/\partial y)_w}{\rho_\infty U_\infty H_e} = \frac{2\rho_w\mu_w}{\rho_\infty G} g'(0) = \frac{g'(0)}{f''(0)} C_f \tag{21}$$

Concerning the influence of cooling, which enters through the boundary-layer functions $f''(0)$ and $g'(0)$, it is seen from Eqs. (2) and (21) in conjunction with Figs. 3 and 4 that it has the usual effect of increasing both C_f and C_h.

The values of $f''(0)$ and $g'(0)$ to be used in Eqs. (19–21) for case 3 correspond to $\lambda = 1$ in Eq. (14), independent of β, and are, therefore, the same for all members of the exponential pressure distribution family Eq. (17). As indicated in Fig. 6, this means that such exponential solutions in fact exist only on cool nonadiabatic

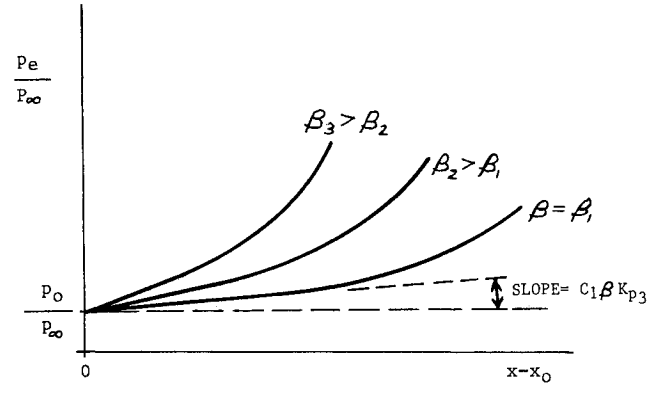

Fig. 5 Mixed ramp-power law pressure distribution for case 4 similarity solutions.

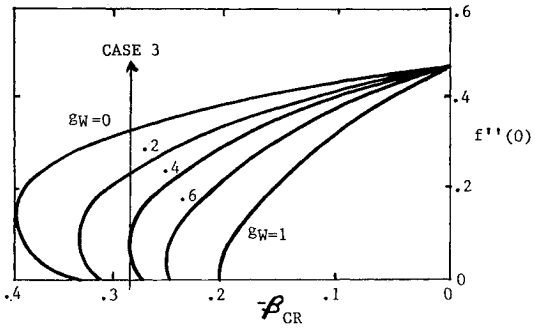

Fig. 6 Realm of case 3 similarity solutions, $\gamma = 1.40$.

walls where $T_w/T_0 < 0.40$ ($\gamma = 7/5$). Within this realm, we further see from Eqs. (19) and (21) that the skin friction and heat transfer in the adverse pressure gradient flow of case 3 actually increase with distance; the flow therefore never separates as it proceeds into the adverse pressure gradient. This important but seemingly paradoxical result is unique to strongly hypersonic flows and can be explained by using the general order of magnitude estimate for a laminar flow that $\tau_w \sim \mu_w U_e/\delta \sim \mu_w U_e/\sqrt{(\mu_w X/\rho_w U_e)} \sim \sqrt{(\rho_w \mu_w/x)} \cdot U_e^{3/2}$. Now, whereas in low-speed constant density flow $\tau_w \sim U_e^{3/2}$ and so by Bernoulli decreases in a region of rising pressure, its behavior in a hypersonic flow with U_e constant and $\rho_w \sim p_e$ is seen to be the opposite owing to the strong streamwise change in density.

Turning to the case 4 solutions for the family of ramp-like pressure distributions Eq. (18), the values of $f''(0)$ and $g'(0)$ to be used in Eqs. (20) and (21) here pertain to $\lambda = \beta$ and, hence, to a much wider range of conditions corresponding to the entire permissible set of β values and wall temperature ratios for nonreversed flows indicated in Figs. 2 and 3. As regards the streamwise variation properties, it is seen from Eqs. (20) and (18) that τ_w also increases in this ramp-like pressure rise when $\beta > 1/2$ and so, here as well, will not separate in the adverse pressure gradient; under this circumstance, the aforementioned effect of $\tau_w \sim \sqrt{p_e}$ predominates over the tendency of τ_w to decrease with increasing x. Since the maximum permissible value of β for $\gamma = 7/5$ is about $0.5\gamma/(\gamma - 1) \approx 1.2$ (see Fig. 2), the special $\beta = 1/2$ situation in which τ_w and $\dot{q}_w$ are constant along the flow is indeed a realizable one within the realm of unique similarity solutions addressed here.

Validation of Results

The author is not aware of any experimental results or exact numerical (N–S) predictions for the present new self-similar pressure distributions that may be used for direct quantitative comparisons. However, there do exist experimental laminar flow data and calculations for strongly hypersonic laminar boundary-layer flows into nonsimilar adverse pressure gradients that lend qualitative support to the present findings. Experiments in 1970 carried out at Imperial College[6] on a cubic compression ramp at $M = 12.2$, a subsequent study of an analogous type of flow by Stollery[7] at Cranfield at $M = 8.2$, and the recent data reported by Holden and Chadwick[8] for a polynomial-shaped ramp at Mach numbers from 10–12 have all shown that the highly cooled hypersonic laminar boundary layer in an adverse pressure gradient indeed thins out and exhibits increasing skin friction and heat transfer as predicted by the present theory. Likewise, an extensive numerical study by Fitzhugh[9] of compressible boundary-layer solutions in a linear adverse pressure gradient has shown exactly the same thing when the external Mach number exceeds 6–7 and the wall is highly cooled, as have the Navier–Stokes calculations reported along with the data of Ref. 8. The present work offers a deeper description of—and explanation for—this seemingly paradoxical but quite real state of affairs: the strongly-hypersonic flow regime contains behavior not accounted for by a traditional low-speed intuition, owing to the dominant thermodynamic effects.

Displacement Thickness

The attendant displacement thickness growth in the strongly hypersonic limit $(\gamma - 1)M_\infty^2 \gg 2$ is approximately equal to the boundary-layer thickness itself and is given by

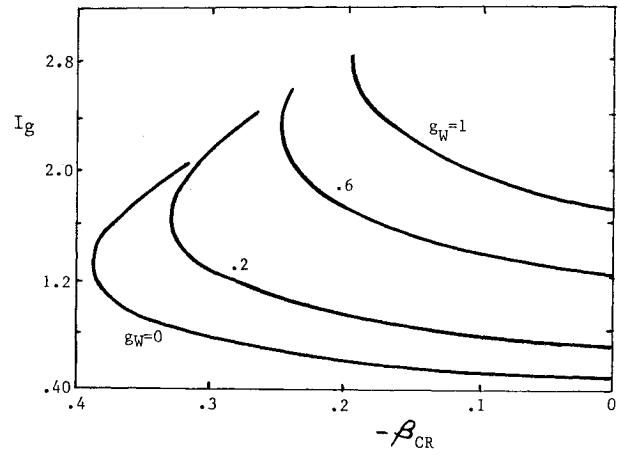

Fig. 7 Values of the displacement thickness integral function.

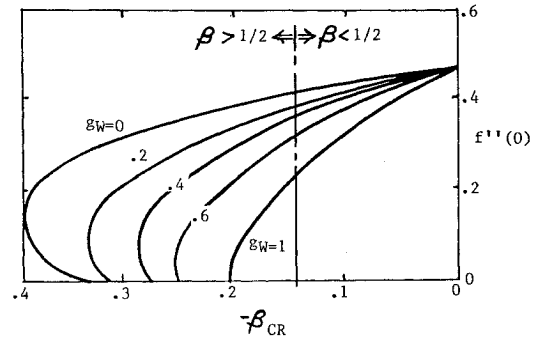

Fig. 8 Divided realm of case 4 solutions, $\gamma = 1.40$.

$$\frac{\delta^*}{L} \equiv \int_0^{\delta/L} \left(1 - \frac{\rho u}{\rho_e u_e}\right) \mathrm{d}\left(\frac{y}{L}\right) \cong \left(\frac{\gamma - 1}{2}\right) \frac{U_\infty G}{\gamma p_e L} \cdot I_g \tag{22a}$$

$$\frac{\delta^*}{L} = \left(\frac{\gamma - 1}{2}\right) M_\infty^2 \sqrt{\frac{2C_w}{Re_L}} I_g$$

$$\cdot \begin{cases} (\beta K_{p_1})^{-\frac{1}{2}} \exp(-\beta \hat{x}/2), & \text{case 3} \qquad (22b) \\ K_{p_3}^{-\beta/2} (p_e/p_\infty)^{(1-2\beta)/2\beta}, & \text{case 4} \qquad (22c) \end{cases}$$

where

$$I_g = \int_0^\infty (g - f'^2)\, \mathrm{d}\eta$$

is a known integral property of the self-similar solutions (values are given in Fig. 7 as a function of T_w/T_0 and β). Equation (22b) predicts in case 3 that the δ^* of this restricted family of nonadiabatic nonseparating flows actually thins out with increasing distance into the rising exponential pressure. As in the preceding discussion, this can be understood from an order of magnitude estimate, $\delta^* \sim \sqrt{(\mu_w x/\rho_w u_e)}$: whereas in low-speed constant density flow, $\delta^* \sim u_e^{-1/2}$ and thus increases in a decelerating flow, a hypersonic boundary layer with u_e constant and $\rho_w \sim p_e$ instead thins out as it proceeds into an adverse pressure gradient. The predicted behavior in case 4 involves a thickening along the flow when $\beta < 1/2$ but a thinning out when $\beta > 1/2$, with δ^* remaining constant along the flow in the special situation $\beta = 1/2$ (see Fig. 8). These different hypersonic regimes of streamwise variation can be understood from the opposing competitive effects of $\delta^* \sim x^{1/2}$ vs $\delta^* \sim p_e^{-1/2}$ also implied by the aforementioned order of magnitude estimate and have an important bearing on the pressure induced by viscous-inviscid interaction as discussed subsequently.

The foregoing displacement thickness distribution, by definition, is directly proportional to the local total mass flow defect associated with the boundary layer (a quantity of practical interest, for example, in the aerodynamic design of engine inlets). In particular, this defect is equal to $\rho_e u_e \delta^*$ where ρ_e is the local inviscid flow density; using

Eq. (22a) plus Eq. (1) and the given values of $G(x)$, this can be expressed in the convenient working form

$$\rho_e u_e \delta^* = \rho_\infty U_\infty L\left(\frac{\gamma-1}{2}\right) M_\infty^2 \sqrt{\frac{2C_w}{Re_L}} I_g \left(\frac{T_\infty}{T_e}\right) \cdot \begin{cases} \sqrt{K_{p_1}/\beta}\exp(\beta\hat{x}/2), & \text{case 3} \quad (23a) \\ \sqrt{(p_e/p_\infty)^{1/\beta}/K_{P_3}^{\beta}}, & \text{case 4} \quad (23b) \end{cases}$$

This defect clearly increases with increasing distance of penetration into the adverse gradient of case 3, and also it reduces along the gradient of case 4 since it is proportional to $p_e^{1/2\beta}$. The expected influence of wall cooling in reducing the defect, owing to the reduction of I_g with T_w/T_0 (Fig. 7), is also evident.

Corresponding Body Shape

It is of obvious interest to establish the body shape that would produce the inviscid pressure distributions associated with these self-similar boundary-layer solutions. We shall do this by means of the well-known tangent wedge approximation of hypersonic flow theory,[3] which to good engineering accuracy links the pressure to the effective body slope according to the analytical relationship

$$\frac{p_e}{p_\infty} \cong 1 + \frac{\gamma}{4}(\gamma+1)K_B^2 + \gamma K_B\sqrt{1+\left(\frac{\gamma+1}{4}\right)^2 K_B^2} \quad (24a)$$

where

$$K_B \equiv M_\infty \sin\theta_{B\text{eff}} = \frac{M_\infty \mathrm{d}y_{B\text{eff}}/\mathrm{d}x}{\sqrt{1+(\mathrm{d}y_{B\text{eff}}/\mathrm{d}x)^2}} \quad (24b)$$

Consistent with the foregoing assumptions, we hereafter continue attention to the strong hypersonic or Newtonian-like limit $K_B^2 \gg 1$ pertaining to either slender or nonslender bodies. Moreover in the present first phase of study where strong viscous interaction is neglected, we take $y_{B\text{eff}} = y_B$ whereupon Eq. (24) provides an inversion relationship in the form of the following nonlinear first-order differential equation governing $y_B(x)$:

$$\frac{\mathrm{d}\hat{y}_B}{\mathrm{d}\hat{x}} \cong \left[f_p \cdot \sqrt{1+\left(\frac{f_p}{2}\right)^2} + \frac{1}{2}f_p^2\right]^{\frac{1}{2}} \quad (25)$$

where $f_p \equiv (2p_e/p_\infty)/\gamma(\gamma+1)M_\infty^2$. Note here that we have taken $p_e \gg p_\infty$ pertaining to the large disturbance limit.

To proceed further, we consider a situation of considerable practical interest in which our adverse pressure gradient body $y_B(x)$ is preceded on $x < x_0$ by a slender constant pressure ramp whose local inviscid flow is strongly hypersonic (see Fig. 9). With y_B measured relative to this ramp, its shape in the initial region $x > x_0$ of the exponential pressure rise (case 3) can be obtained by taking $f_p \ll 1$ in Eq. (25); using Eq. (17) and then integrating, we thus find for case 3 that

$$\hat{y}_B(\hat{x}) \cong \int_{\hat{x}_0}^{\hat{x}} f_p^{\frac{1}{2}}\,\mathrm{d}\hat{x} = \sqrt{\frac{4p_e(x_0)/p_\infty}{\gamma(\gamma+1)\beta^2 M_\infty^2}} \cdot \left[e^{(\beta/2)(\hat{x}-\hat{x}_0)} - 1\right] \quad (26)$$

where we have identified $K_{p_1}\exp(\beta\hat{x}_0) = p_e(x_0)/p_\infty$, the hypersonic pressure ratio on the ramp. As expected, this shape is an exponential curve following the pressure (Fig. 9a). Turning to the pressure rise of Eq. (18) for case 4, its initial body shape for $x > x_0$ is obtained by a comparable integration to be

$$\hat{y}_B(\hat{x}) \cong \sqrt{\frac{4p_e(x_0)/p_\infty}{\gamma(\gamma+1)C_1^2(2-\beta)^2 M_\infty^2}} \cdot \left\{[1+C_1(1-\beta)(\hat{x}-\hat{x}_0)]^{(2-\beta)/2(1-\beta)} - 1\right\} \quad (27)$$

which is an upward-curving ramp shape of initial slope proportional to $C_1(2-\beta)$ as illustrated in Fig. 9b.

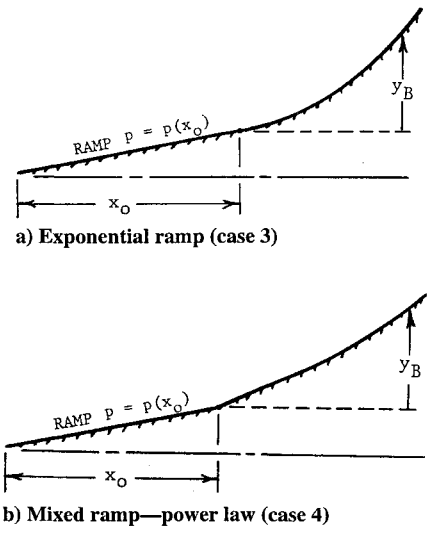

Fig. 9 Compression inlet shapes employing the new similarity solutions.

Induced Pressure Field

The viscous displacement effect, by enhancing the effective local body slope according to

$$\frac{\mathrm{d}y_{B\text{eff}}}{\mathrm{d}x} = \frac{\mathrm{d}y_B}{\mathrm{d}x} + \frac{\mathrm{d}\delta^*}{\mathrm{d}x} \quad (28)$$

in the hypersonic limit,[3] serves to induce an additional pressure field along the body, which can be important at very high-altitude flight conditions. In the present paper, we estimate this pressure increment for situations where it is small to moderate and, thus, does not significantly back-effect $\delta^*(x)$ itself, the so-called weak interaction case. This situation applies to many high-speed inlet flows of practical interest.[8]

To carry out this interactive analysis for a flow that already possesses a significant inviscid pressure gradient, we draw on a generalized treatment of this situation for weak interactions given by Hayes and Probstein.[3] Using in part the slender body version of the tangent wedge relationship [Eq. (24)] together with Eq. (28), this work showed that the increment in local pressure (relative to the purely inviscid bare body value $p_{e_{\text{bare}}}$) due to viscous interaction is given by

$$\frac{p_e - p_{e_{\text{bare}}}}{P_\infty} \cong \gamma M_\infty \mathcal{L}\left(\frac{\mathrm{d}\delta^*}{\mathrm{d}x}\right) \quad (29)$$

where in the present $K_B^2 \gg 1$ limit

$$\mathcal{L} \cong (\gamma+1)M_\infty\left(\frac{\mathrm{d}y_B}{\mathrm{d}x}\right) \quad (30)$$

and where the $\mathrm{d}\delta^*/\mathrm{d}x$ values here are to be obtained from differentiation of Eq. (22). At this stage, it already can be seen from these relations that the interactive pressure change is proportional to $M_\infty^3\sqrt{(C_w/Re_L)} \sim \bar{\chi}$ (the viscous interaction parameter).

Focusing specifically on the compressive inlet ramp set up of Fig. 9 with $K_B^2 \gg 1$ and $\mathrm{d}y_B/\mathrm{d}x \cong \sqrt{(2p_e/p_\infty\gamma(\gamma+1)M_\infty^2)}$ [Eq. (25)] with $p_e = p_{e_{\text{bare}}}$ for weak interaction, Eqs. (29) and (30) yield, in general, for this limit

$$\frac{p_e - p_{e_{\text{bare}}}}{p_\infty} \cong \sqrt{2\gamma(\gamma+1)}\frac{p_{e_{\text{bare}}}}{p_\infty} M_\infty \frac{\mathrm{d}\delta^*}{\mathrm{d}x} \quad (31)$$

Then in case 3, substitution of Eqs. (22) and (26) yields

$$\frac{p_e - p_{e_{\text{bare}}}}{p_\infty} \cong -\left(\frac{\gamma-1}{2}\right)\sqrt{\gamma(\gamma+1)\beta} I_g \bar{\chi} \quad (32)$$

This result predicts that the relative interactive pressure change is, in fact, a uniform reduction along the entire length of the exponential

bare body pressure rise, evidently due to the thinning out of δ^* [see Eq. (22b)] that occurs in this case. Turning to case 4, use of Eqs. (22) and (27) in Eq. (31) gives

$$\frac{p_e - p_{e_{\text{bare}}}}{p_\infty} \cong -\left(\frac{\gamma-1}{2}\right)\sqrt{\frac{\gamma(\gamma+1)}{K_{p_3}}} \times I_g\left(\frac{2\beta-1}{1-\beta}\right)\bar{\chi}\cdot[1+C_1(1-\beta)(\hat{x}-\hat{x}_0)]^{-\frac{1}{2}} \tag{33}$$

Here, it is seen that the interactive pressure rise vanishes exactly in the special case $\beta = \frac{1}{2}$ because δ^* here is constant along the flow [Eq. (22c)], whereas for $\beta > \frac{1}{2}$ it becomes a reduction that decreases along the length of this ramp-like flow. In both cases, Eqs. (32) and (33) show that the weak interactive pressure effect is directly proportional to $\bar{\chi}$ and to I_g; thus (see Fig. 6) wall cooling significantly reduces the effect as expected.

Total Pressure Loss Profile Across Boundary Layer

The distribution of the total pressure loss across the boundary layer is of general interest in experimental work and of particular interest to inlet aerodynamics since turbomachinery performance is very sensitive to the total head profile. A revealing working relationship for $P_0(y)$ in the present self-similar flows can be readily obtained from first principles as follows. By definition

$$\frac{P_0(y)}{P_{0_e}} = \left[\frac{2+(\gamma-1)M^2(y)}{2+(\gamma-1)M_e^2}\right]^{\gamma/(\gamma-1)} \tag{34}$$

where, in turn, the Mach number profile of the boundary layer is $M^2 = u^2/\gamma RT = M_e^2 f'^2/(T/T_e)$ or, using Eq. (8),

$$M^2(y) = M_e^2(f')^2 \Big/ \left[g + \left(\frac{\gamma-1}{2}\right)M_e^2(g-f'^2)\right] \tag{35}$$

It is important to note that the first term in the denominator here must be retained near the boundary-layer edge (f', g near unity) even for $M_e^2 \gg 1$. Then substituting Eq. (35) into Eq. (34), we find after some algebra the interesting general relationship that

$$\frac{P_0(\eta)}{P_{0e}} = \left\{g \Big/ \left[g + \left(\frac{\gamma-1}{2}\right)M_e^2(g-f'^2)\right]\right\}^{\gamma/(\gamma-1)} \tag{36}$$

Equation (36) links the total head directly to the velocity and total enthalpy profiles across the boundary layer. Typical such profiles for the present similarity solutions at several wall temperature ratios are shown in Fig. 10. Inspection of these curves in conjunction with Eq. (36) clearly brings out that very large total head losses occur across the inner portion of a highly cooled hypersonic boundary layer; for example, at the wall, Eq. (36) predicts for strongly hypersonic flow that $P_{0w}/P_{0e} \cong [2/(\gamma-1)M_e^2]^{\gamma/(\gamma-1)}$, which is less than 0.01 at $M_e \geq 4.4$.

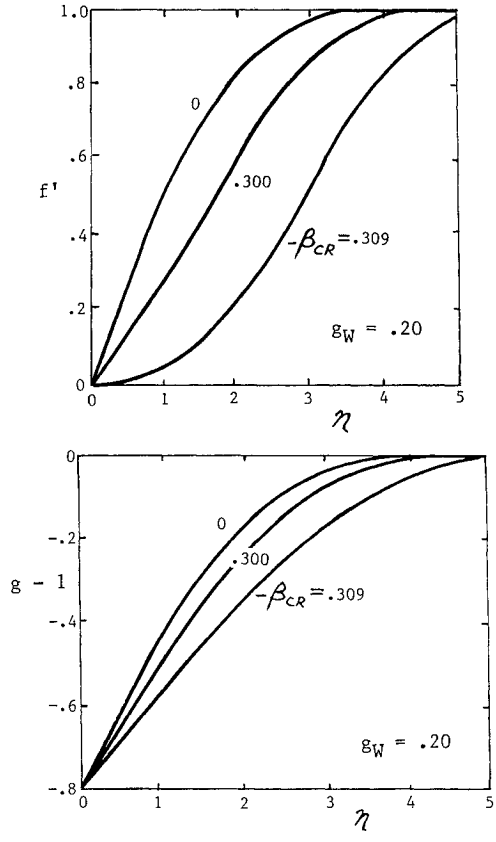

Fig. 10 Typical velocity and total enthalpy profiles for the present similarity solutions.

Applications to High-Speed Inlet Flows

It would appear the present work could benefit the aerodynamic design of hypersonic inlets in a number of ways. First, the new similarity solutions offer exact results for two well-defined body shape families that can be used to validate the purely numerical predictions of CFD codes applied to the difficult realm of adverse pressure gradient flows. As an example, the skin friction, heat transfer, and displacement thickness distributions for a case 3, $\beta = 1$ pressure distribution on a $T_w = 0.20T_0$ cold wall at Mach 14 with a 10-deg pre-exponential ramp angle [$p_e(x_0)/p_\infty = 9.67$ for $\gamma = 1.4$] is shown in Fig. 11. Second, the solutions provide the foundation of a cost-effective engineering analysis method based on the local similarity approximation,[10] which should yield reasonably accurate skin friction, heat transfer, and induced pressure field predictions for the highly cooled hypersonic flows expected in practice. Third, the present solutions would serve well as initializing upstream conditions for a subsequent purely numerical solution farther downstream into the actual engine inlet diffuser. Such initial boundary-layer profiles would already include the heat transfer and adverse pressure gradient effects on the inlet forebody. Fourth, the present results provide a basis for designing more efficient inlet body shapes and carrying out various optimization studies. For example, in the former category, we have shown that several inlet ramp shapes yield nonseparating hypersonic boundary layer flow even with a significantly adverse streamwise pressure gradient. Regarding the latter, the present results would enable the design of a minimum length type of inlet along which the skin friction is maintained at virtually zero by the suitable choice of the wall temperature level (for example, by the $T_w/T_0 \approx 0.40$ situation in case 3 or choosing $\beta = \beta_{\text{sep}}(T_w/T_0)$ from Fig. 2 in case 4). Another such application would be an inlet designed for friction and zero viscous interaction-induced pressure, defined by the $\beta = \frac{1}{2}$ member of the case 4 family of shapes.

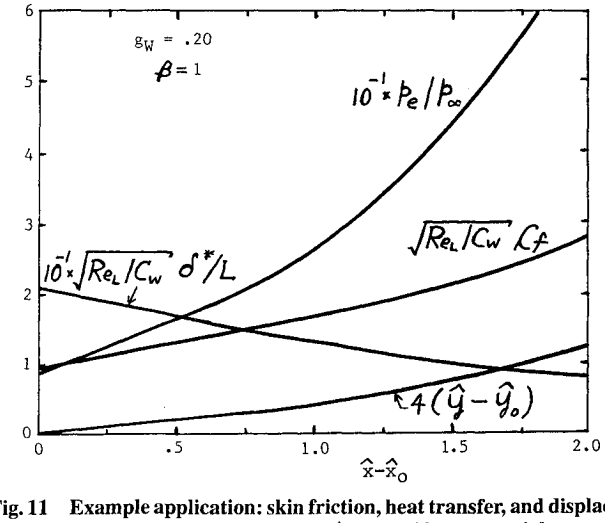

Fig. 11 Example application: skin friction, heat transfer, and displacement thickness for an $M_{(\infty)} = 14$, $T_w/T_0 = 0.20$ exponential pressure distribution with $\beta = 1$, $\gamma = 1.40$.

Concluding Remarks

The present investigation has identified and evaluated two new families of similarity solutions pertaining to hypersonic boundary layers in adverse pressure gradients. These involve either an exponential or curved-ramp type of pressure rise along which, owing to the strongly hypersonic flow conditions assumed, the boundary layer does not necessarily separate. The results may thus be valuable in achieving more efficient aerodynamic designs of high-speed engine inlets.

Several extensions of the work would appear desirable and feasible. These include the treatment of the axisymmetric case via the use of the Mangler transformation in the original formulation (this has in fact already been done) and the addition of wall suction or blowing effects whose streamwise distributions are compatible with similarity, in order to assess the influence of body ablation or boundary-layer control, respectively, on adverse pressure gradient boundary layers approaching an inlet. Furthermore, it would be of great interest for very high-altitude hypersonic flight conditions to extend the present treatment of weak viscous-inviscid interaction ($\bar{\chi} < 1$) into the strong interaction regime where $\bar{\chi} \gg 1$, wherein the back effect of the resulting pressure change on δ^* itself plus C_f and C_h cannot be neglected and must therefore be treated simultaneously in a coupled manner. The resulting changes in the associated effective body shape and nonseparating skin friction behavior predictions would be particularly interesting.

References

[1]Mirels, H., "Hypersonic Flow Over Slender Bodies with Power Law Shocks," *Advances in Applied Mechanics VII*, Academic, New York, 1962, pp. 1–54.

[2]Coles, J. D., and Aroesty, J., "Hypersonic Similarity Solutions for Airfoils Supporting Exponential Shock Waves," *AIAA Journal*, Vol. 8, No. 2, 1970, pp. 308–315.

[3]Hayes, W. D., and Probstein, R. F., *Hypersonic Flow Theory*, Academic, New York, 1959.

[4]Stewartson, K., *Theory of Laminar Boundary Layers in Compressible Fluids*, Oxford Univ. Press, London, 1964.

[5]Cohen, C. R., and Reshotko, E., "Similar Solutions for the Compressible Laminar Boundary Layer with Heat Transfer and Pressure Gradient," NACA Rept. 1293, 1956.

[6]Mohammadian, S., "Hypersonic Boundary Layers in Strong Pressure Gradients," Ph.D. Thesis, Imperial College, London Univ., London, 1970.

[7]Stollery, J. L., "Some Aspects of Shock Wave-Boundary Layer Interaction Relevant to Intake Flows," *Hypersonic Combined Cycle Propulsion*, AGARD Conf. Proc. 479, 1994.

[8]Holden, M. S., and Chadwick, K. M., "Studies of Laminar, Transitional, and Turbulent Hypersonic Flows over Curved Compression Surfaces," AIAA Paper 95-0093, Jan. 1995.

[9]Fitzhugh, H. A., "Numerical Studies of the Laminar Boundary Layer for Mach Numbers up to 15," *Journal of Fluid Mechanics*, Vol. 36, Pt. 2, 1969, pp. 347–366.

[10]Moore, F. K., "Local Similarity in Steady Flow," *Theory of Laminar Flows*, Princeton Univ. Press, Princeton, NJ, 1964, pp. 483–502.